RSC Publishing Faraday Discussions

Electrospray ionization photoelectron spectroscopy of cryogenic [EDTA•M(II)]2− complexes (M = Ca, V−Zn): electronic structures and intrinsic redox properties

Journal:	*Faraday Discussions*
Manuscript ID	FD-ART-11-2018-000175
Article Type:	Paper
Date Submitted by the Author:	12-Nov-2018

Complete List of Authors:	Yuan, Qinqin; Dalian Institute of Chemical Physics, Chinese Academy of Sciences, Kong, Xiang-Tao; Dalian Institute of Chemical Physics, State Key Laboratory of Molecular Reaction Dynamics Hou, Gao-Lei; Eidgenossische Technische Hochschule Zurich Departement Chemie und Angewandte Biowissenschaften, Laboratory of Physical Chemistry Jiang, Ling; Dalian Institute of Chemical Physics, State Key Laboratory of Molecular Reaction Dynamics Wang, Xue-Bin; Pacific Northwest National Laboratory, Physical Sciences Division

Electrospray ionization photoelectron spectroscopy of cryogenic [EDTA•*M*(II)]$^{2-}$ complexes (*M* = Ca, V−Zn): electronic structures and intrinsic redox properties

Qinqin Yuan,[#1,2,3,§] Xiang-Tao Kong,[#2] Gao-Lei Hou,[1] Ling Jiang,*[2] and Xue-Bin Wang*[1]

[1]Physical Sciences Division, Pacific Northwest National Laboratory, 902 Battelle Boulevard, P. O. Box 999, MS K8-88, Richland, Washington 99352, USA

[2]State Key Laboratory of Molecular Reaction Dynamics, Dalian Institute of Chemical Physics, Chinese Academy of Sciences, 457 Zhongshan Road, Dalian 116023, China

[3]University of Chinese Academy of Sciences, 19A Yuquan Road, Beijing 100049, China

*E-mail address: ljiang@dicp.ac.cn (L.J.); xuebin.wang@pnnl.gov (X.B.W.).

[#]These authors contributed equally to this work

[§]visiting student supported via PNNL alternate sponsored fellowship program

Abstract

We report here a systematic photoelectron spectroscopy (PES) and theoretical study of divalent transition metal (TM) EDTA complexes [EDTA•*TM*(II)]$^{2-}$ (*TM* = V − Zn), along with the Ca(II) species for comparison. Gaseous TM dianions (*TM* = Ca, Mn, Co, Ni, Cu and Zn) were successfully generated via electrospray ionization, and their PE spectra, with 157, 193, and 266 nm photons, are obtained at 20 K. The spectrum of each TM complex shows an extra peak at the lowest electron binding energy (eBE), compared to that of [EDTA•Ca(II)]$^{2-}$. DFT calculations indicate hexacoordinated metal-EDTA binding motif for all complexes, from which the vertical detachment energies (VDEs) are calculated and agree well with the experimental values. The calculations further predict negative or very small VDEs for TM (II) = V, Cr, and Fe, providing a rational explanation why these three dianionic species are not observed in the gas phase. Direct spectral comparison, electron spin density differences, and MO analyses indicate that the least bound electrons are derived from TM d electrons with appreciable ligand contributions, in contrast to [EDTA•Ca(II)]$^{2-}$, in which the detachment is entirely derived from the ligand. The extent of ligand modulation, *i.e.*, non-innocence of EDTA ligand in oxidation process are found to vary across the 3rd row of TMs. Comparing gas-phase VDEs of [EDTA•*TM*(II)]$^{2-}$ with the 3rd ionization potentials of TMs and solution phase oxidation potentials reveals intrinsic correlations among these three quantities, with the deviations being largely modulated by the ligand participation. The detailed microscopic information of their intrinsic electronic structures and bonding motifs obtained in this work will help better understand the rich redox chemistries of these ubiquitous species under diverse environments. The present work along with our previous studies indicates PES coupled with electrospray ionization is a unique ion spectroscopic tool that not only provides intrinsic electronic structure and bonding information of redox species important in solutions, but also can predict the related electron transfer chemistries with quantitative capability.

Introduction

Metal organic complexes have been extensively investigated as models of metalloenzyme active sizes, as enzyme inhibitors, and DNA cleavage agents.[1-5] It has been found that chelating ligands can significantly modulate redox behavior of metal ions and influence DNA nuclease activities. As one of the most common organic ligands, ethylenediaminetetraacetate ($EDTA^{4-}$), the conjugate base of an aminopolycarboxylic acid, has "bifunctional chelating groups" of carboxylate and amine groups, and can chelate with almost every metal cation in the Periodic Table using its two nitrogen and four oxygen atoms to form thermodynamically favorable [EDTA•M] complexes. Diverse metal-specific biological and medical functions of divalent metal chelate complexes have been recognized,[6-10] and the related redox potentials under physiologically relevant conditions have been estimated.[5]

A variety of analytical methods have been employed to characterize metal EDTA complexes in solutions[11-17] and crystals[18-23]. Due to the complication of bulk environments, and, in particular, the influences of pH value in solutions, unambiguous coordination motifs between EDTA and various metals are still lacking, and remain considerably uncertain.[13,15,16] Gas-phase ion spectroscopy coupled with electrospray ionization and in combination with quantum chemical calculations has been demonstrated as a powerful technique to obtain intrinsic geometries and electronic structures of exotic species, intermediates, and microsolvated clusters from solutions without bulk perturbations.[24-33] Because photodetachment is a process involving ejection of an electron from anionic species, analogous to a half electron transfer reaction (due to no electron acceptor),[34] explicit electronic structure information mimicking the oxidation process of redox species is encoded in the resulting photoelectron (PE) spectrum, in which the electron binding energy (eBE) derived from the 1st spectral band with the lowest eBE correlates to the intrinsic oxidation potential. Our recent study on a series of EDTA trivalent metal complexes $[EDTA•M(III)]^-$ revealed distinctly different PE spectral pattern for transition metal complexes with d electrons (M = V−Co) compared to those without d electrons (M = Al, Sc), which provided a molecular-level rationale to understand the special redox behavior of vanadium species in biological cells.[35] Given the fact that EDTA divalent metal complexes $[EDTA•M(II)]^{2-}$ are ubiquitous and exhibit rich redox chemistries under diverse environments,[5-

[10] herein, we conducted a systematic investigation by employing electrospray ionization photoelectron spectroscopy (PES) and theoretical modelling on a series of such complexes across the 3rd row metals (*M* = Ca, V− Zn) to probe EDTA−M binding motifs, to obtain their geometries and intrinsic electronic structures, and to examine the metal-specific eBE variation and how well the eBE trend is correlated with redox potentials measured in solutions.

Experimental methodology

The experiments were carried out using the PNNL size-selective, cryogenic, electrospray ionization PES instrument.[28] $[EDTA•Ca(II)]^{2-}$and $[EDTA•Cu(II)]^{2-}$ dianions were produced directly by spraying into vacuum 1.0 mM solutions of EDTA calcium disodium salt and EDTA copper(II) disodium salt dissolved in a mixture of H_2O/CH_3CN (1:3) solvents, respectively. $[EDTA•Mn(II)]^{2-}$ was generated from spraying 1.0 mM aqueous acetonitrile solution of manganese(III) acetate dihydrate and disodium EDTA salts, where a disproportionation reaction occurred. In order to produce all other dianionic complexes $[EDTA•M(II)]^{2-}$, 1.0 mM aqueous acetonitrile solutions of mixed MCl_2 and EDTA disodium salts were prepared and sprayed.

The generated dianionic complexes were guided by two RF only quadrupoles and a 90º bender into a cryogenic 3D ion trap, where they were accumulated and collisionally cooled with buffer gas (20% H_2 balanced in helium) for 20−100 ms. In the current experiments, the ion trap was operated at 20 K to minimize appearance of extra spectral features due to hot bands and improve energy resolution. The cryogenic anions were then pulsed out into the extraction zone of a time-of-flight (TOF) mass spectrometer at a 10 Hz repetition rate, and the desired dianions were each mass-selected and decelerated before being photodetached in the interaction zone with a laser beam. Three different laser wavelengths, 266 nm (4.661 eV from an Nd:YAG laser), 193 nm (6.424 eV from an ArF laser), and 157 nm (7.867 eV from an F_2 laser), were used for photodetachment. All lasers were operated at 20 Hz repetition rate with the ion beam off at alternating laser shots, affording shot-by-shot background subtraction. Photoelectrons were collected at ~100% efficiency with a magnetic bottle and analyzed in a 5.2 m long electron flight tube. The resultant TOF photoelectron spectrum was converted into electron kinetic energy (eKE) spectrum, calibrated by the known spectra of I^-[36], $OsCl_2^-$[37] and $Au(CN)_2^-$[38]. The electron binding energy spectra, presented in the manuscript, were obtained by subtracting the kinetic

energy spectra from the detachment photon energies. The electron energy resolution was about 2% (i.e., ~20 meV for 1 eV kinetic energy electrons).

Theoretical methodology

Density functional theory (DFT) calculations using PBE0, B3LYP, MN12SX, BP86, and MN15 functionals with the 6-311+G(d,p) basis set for all atoms, were carried out for $[EDTA•M(II)]^{2-}$ (M = Ca, V−Zn). Structures were optimized using tight convergence criteria without any symmetry restrictions. Harmonic vibrational frequency analyses were performed to confirm that all structures were real minima. All relative energies reported include zero-point energy corrections. Theoretical vertical detachment energies (VDEs) are calculated as the electronic energy differences between the singly charged anions and the corresponding dianions both at the optimized dianion's geometries. Table S1† in the supporting materials compares the experimental VDEs with theoretical VDEs, calculated using these five different functionals for $[EDTA•M(II)]^{2-}$ (M = Ca, Mn, Co, Ni, Cu and Zn). It can been seen that functional MN12SX yields best VDEs in comparison to the experiments over others for the complexes containing 3d electrons, while M06-2X is a good choice to calculate VDE for those without 3d electrons, i.e., for the Ca(II) case. A similar preference of different functionals was found in our recent study for trivalent metal EDTA systems.[35] In this work, for the convenience of discussion, we present the MN12SX results for all $[EDTA•M(II)]^{2-}$ (M = Ca, V−Zn) in the main text unless otherwise noted. Different spin states were also considered for the complexes with unpaired 3d electrons for M = Mn, Co and Ni in Table S2†, which suggests that high spin states are more stable than low spin states by at least 1.0 eV in energy. The excited state energies of the singly charged anions, accessible via photodetaching the corresponding dianions, were calculated using time-dependent DFT (TD-DFT) at the dianion's geometries. All quantum chemical calculations were performed using the Gaussian 09 program suite.[39]

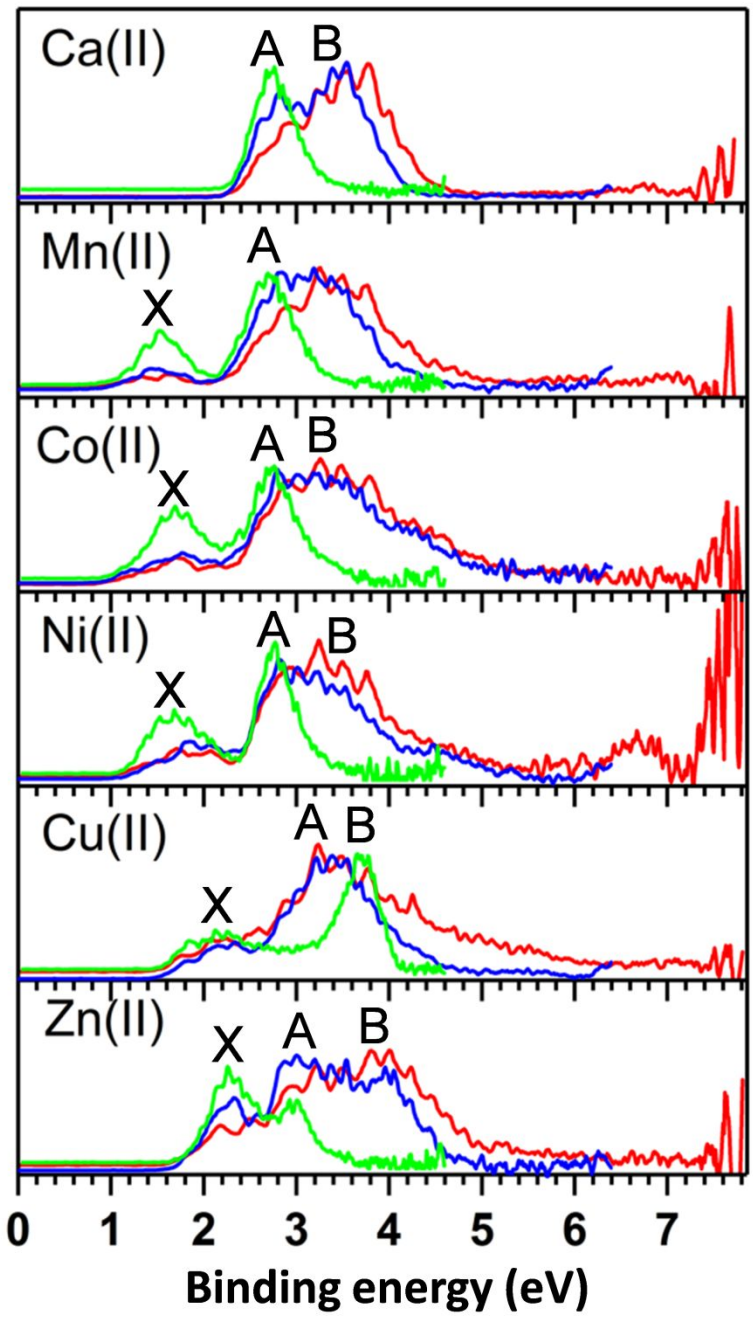

Fig. 1 20 K photoelectron spectra of [EDTA•*M*(II)]$^{2-}$ (*M* = Ca, Mn, Co, Ni, Cu, and Zn) at 157 nm (7.867 eV, red), 193 nm (6.424 eV, blue), and 266 nm (4.661 eV, green).

Table 1 Experimental / calculated vertical detachment energies (VDEs), and experimental repulsive Coulomb barriers (RCB) for [EDTA•*M*(II)]$^{2-}$.

[EDTA•M]$^{2-}$	Ca(II)	V(II)	Cr(II)	Mn(II)	Fe(II)	Co(II)	Ni(II)	Cu(II)	Zn(II)
Expt. VDE (eV)[a]	2.70(10)			1.15(10)		1.70(10)	1.73(10)	1.78(10)	2.20(20)
Calc. VDE (eV)[b]	2.33 (2.90)[c]	-0.42	0.16	1.16	0.64	1.64	1.63	1.66	2.08
Expt. RCB (eV)	~2.0			~2.0		~2.0	~1.9	~2.0	~2.0

[a]Numbers in parentheses represent experimental uncertainties in the last digits. [b]MN12SX/6-311+G(d,p) VDEs, unless otherwise noted. [c]The calculated VDE for Ca(II) in parenthesis is the M06-2X /6-311+G(d,p) value.

Experimental results

We have made intentional efforts to conduct a holistic study on [EDTA•*M*(II)]$^{2-}$ complexes across the third-row transition metal (*M* = V−Zn). [EDTA•*M*(II)]$^{2-}$ type of dianions were generated abundantly via electrospray ionization for *M* = Mn, Co, Ni, Cu, and Zn, but not for *M* = V, Cr and Fe. For the latter three metals, [EDTA•*M*(III)]$^{-}$ were observed instead, presumably due to the fact that the corresponding *M*(II) dianions were very sensitive to oxidation, and easily oxidized to the *M*(III) singly charged complexes by adventitious O_2 during electrospray. The PE spectra of [EDTA•*M*(III)]$^{-}$ (V, Cr, Fe) were reported in our previous publication.[35] This 'negative' portion of the experiments does, however, suggest that [EDTA•V(II)/Cr(II)/Fe(II)]$^{2-}$ should have very small if not negative VDE values, which is confirmed by our theoretical calculations as shown in the next sections.

Photodetachment phtotoelectron spectroscopic measurements of [EDTA•*M*(II)]$^{2-}$ (*M* = Ca, Mn, Co, Ni, Cu, and Zn) were carried out at 20 K using 157, 193, and 266 nm photons, and the results are illustrated in Figure 1. The 157 nm PE spectrum of [EDTA•Ca(II)]$^{2-}$ shows a broad band at the eBE range of 2.4 to 4.6 eV consisting of two discernible features A & B, while those of transition metal (*TM* = Mn, Co, Ni, Cu, and Zn) complexes each possesses main spectral bands A & B similar to that in the Ca case. In addition, a weak band X at low eBE is seen in each Mn, Co, Ni, Cu, and Zn complex spectrum, whose position increases with *TM* atomic number.

The PE spectrum of each complex at 193 nm looks similar to that at 157 nm, with the intensity of feature A slightly increased; while at 266 nm, only feature A is observed for *M* = Ca, features X & A for *M* = Mn, Co, Ni, Zn, and features X & B for *M* = Cu (Figure 1).

Repulsive Coulomb barrier (RCB), a general feature in photodetachment of multiply charged anions (MCAs), leads to a hallmark in any PE spectrum of MCA, resulting in truncating any PE signals with eKE of electrons less than the height of RCB and significantly reducing electron signals for electrons with eKE ≈ RCB (Fig. S1).[40,41] The cutoffs and intensity variation of spectral features observed at different wavelengths for each species in Figure 1 are direct results of their dianionic nature of each complex. On the one hand, at 193 nm, the majority of feature B is seen for each species, indicating the RCB should be less than 2.4 eV (by subtracting 4.0 eV from 6.4 eV). On the other hand, at 266 nm, feature A is seen either red-shift or its intensity appreciably reduced, suggesting the RCB should be larger than 1.6 eV (by subtracting 3.0 eV from 4.6 eV). A more close examination of the spectral cutoff position at 193 and 266 nm leads to an approximated 2.0 eV RCB for these complexes (Table 1). It is worth pointing out that feature B for each complex should not be seen at 266 nm because of the RCB cutoff effect. However, a strong peak at the B position in the Cu(II) spectrum exhibits at 266 nm (Figure 1), which is most likely due to resonant autodetachment.[42]

The first spectral band for [EDTA•Ca(II)]$^{2-}$ is feature A, which has no 3d electrons in the metal Ca (II) center, while that for each [EDTA•*TM*(II)]$^{2-}$ species containing 3d electrons is feature X. Similar observation was reported in the PES study of [EDTA•*M*(III)]$^{-}$.[35] The experimental VDE for [EDTA•*M*(II)]$^{2-}$ was measured from the maximum of the first peak in each spectrum, and it is 2.70 ± 0.10 (Ca), 1.15± 0.10 (Mn), 1.70 ± 0.10 (Co), 1.73 ± 0.10 (Ni), 1.78 ± 0.10 (Cu), and 2.20 ± 0.20 eV (Zn) (Table 1), respectively.

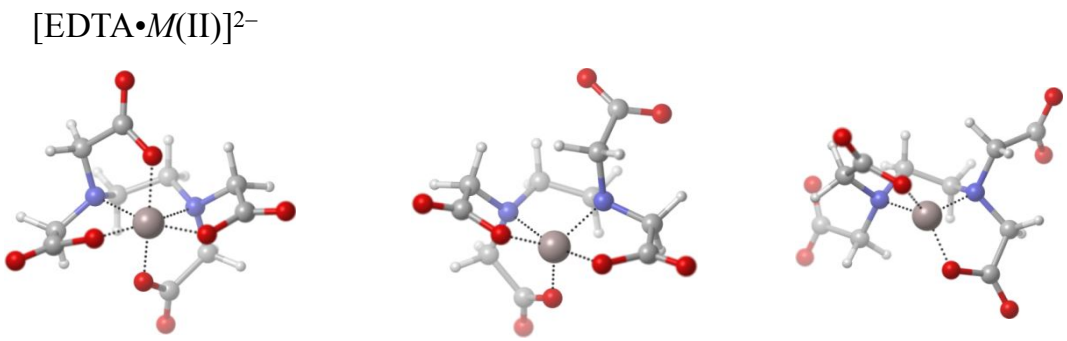

Fig. 2 Three binding motifs for [EDTA•*M*(II)]$^{2-}$ complexes with hexa-, penta- and tetra coordination (H, light grey; C, grey; O, red; N, blue; M, light brown).

Theoretical results and discussion

A. Optimized structures of [EDTA•*M*(II)]$^{2-}$

Three metal ligand binding motifs, including hexadentate (Iso A), pentadentate (Iso B) and tetradentate (Iso C) EDTA metal complexes, were optimized and presented in Figure 2. Our calculations show that the quasi-octahedral type structure with hexadentate ligand (Iso A) is the most stable isomer for all metal complexes (Table S3, ESI†). Penta-coordinated Iso B is calculated to be the next lowest energy isomer, being 0.75 (Ca), 0.73 (V), 0.44 (Cr), 0.42 (Mn), 0.25 (Fe), 0.15 (Co), 0.34 (Ni), 0.06 (Cu) and 0.23 eV (Zn) higher in energy than Iso A. The binding motif of tetra-coordinated Iso C is found to be much less favorable, by 0.8 eV compared to Iso A for all species except for Cu, which is 0.21 eV higher in energy (Table S4, ESI†).

Since isomers A and B are close in energy, it is instructive to calculate the transition barriers between these two isomers, to help estimate the existence of one or both isomers in the experiments. Our DFT calculations show that there exist substantial barriers between Iso A and Iso B for the Ca, Mn, Co, Ni, and Zn complexes, i.e., 1.34 (Ca), 1.09 (Mn), 0.86 (Co), 1.05 (Ni), and 0.91 eV (Zn), while an appreciably smaller barrier of 0.29 eV for the Cu(II) species (Table S4). The above energetic and barrier analyses suggest the dominance of the hexadentate Iso A for [EDTA•*M*]$^{2-}$ (*M* = Ca, Mn, Co, Ni and Zn) in the experiments. The coexistence of the nearly

isoenergetic isomers A and B is likely for [EDTA•Cu(II)]$^{2-}$, because its calculated spectrum also matches to the part of the observed spectrum (vide infra).

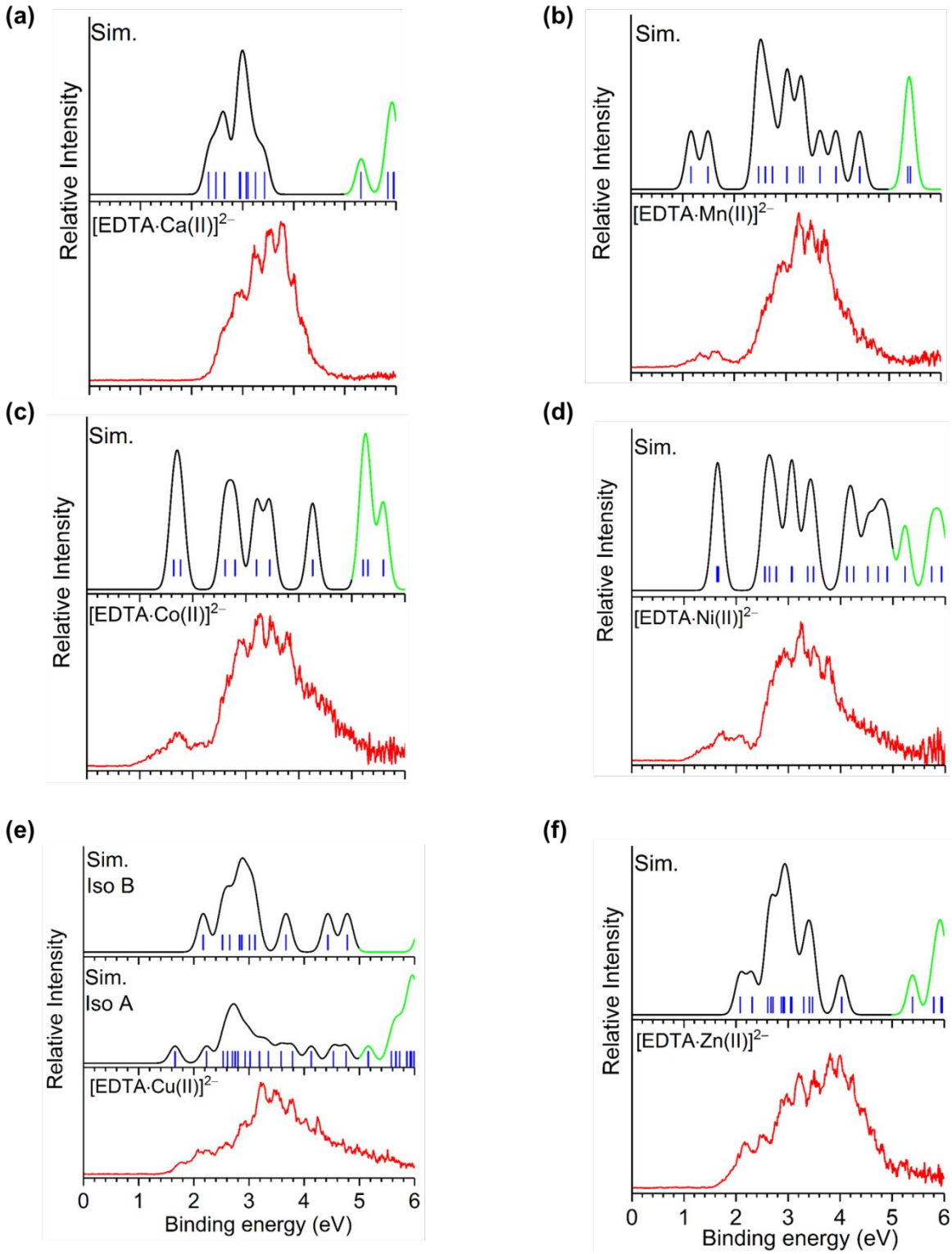

Fig. 3 MN12SX simulated PE spectra (black and green) and the stick spectra (blue) of the lowest isomers for [EDTA•*M*(II)]$^{2-}$ complexes (Iso A for *M* = Ca, Mn, Co, Ni, and Zn; Iso A and B for Cu), in comparison with the corresponding experimental spectra at 157 nm (red). The simulated stick spectrum for each complex was generated using the calculated VDE and TDDFT excitation energies, and the simulated spectrum was obtained by convoluting the stick spectrum with Gaussian functions of 0.1 eV full widths at half maximum for each stick. The predicted spectral bands at high eBE side (green) will not be observed in experiments due to the spectral cutoff by repulsive Coulomb barriers.

B. Calculated VDEs and simulated spectra

Table 1 lists the MN12SX / 6-311+G(d,p) VDEs of all [EDTA•*M*(II)]$^{2-}$ complexes, as well as the M06-2X / 6-311+G(d,p) VDE for the Ca species, based on the most stable quasi-octahedral isomer A. Comparing to the experimental value for the Ca complex, the M06-2X functional overestimates the VDE by 0.2 eV, while MN12SX underestimates the VDE by 0.37 eV. For all TM complexes, the agreement in-between the experimental and MN12SX VDEs is excellent, i.e. 1.15/1.16 (Mn), 1.70/1.64 (Co), 1.73/1.63 (Ni), 1.78/1.66 (Cu) and 2.20/2.08 eV (Zn). Consequently, the MN12SX / 6-311+G(d,p) methodology was also utilized to predict the VDE values for the three [EDTA•*M*(II)]$^{2-}$ (*M* = V, Cr, Fe) complexes that could not be generated in our experiments. As shown in Table 1, the calculated VDEs, −0.42, 0.16, and 0.64 eV for V, Cr and Fe, respectively, are either negative or very small, suggesting that these dianionic complexes are readily oxidized, consistent with the absence of these three complexes in the present experiments.

Figure 3 shows the comparison of the TD-DFT simulated spectra of the lowest isomers for *M*(II) = Ca, Mn, Co, Ni, Cu, and Zn to the experimental ones. The extra spectral peaks near the photon energy limit (green) in the simulated spectra are not expected to be observed in the experiments, due to the RCB cutoff for photodetaching MCA. It can be seen from Figure 3 that the predicted band positions and overall pattern calculated from the lowest energy Iso A for each species match the experimental spectrum reasonably well, except for [EDTA•Ca(II)]$^{2-}$, in which the simulated spectrum is seen to shift to the low eBE side. This is because, as discussed above, functional MN12SX underestimates the VDE of the Ca species. The good agreement between

the simulated and experimental spectra strongly suggests that isomer A, the quasi-octahedral structure with a hexadentate EDTA largely contributes to the experiment for each complex. In the case of $[EDTA•Cu]^{2-}$, it is likely that the nearly degenerate Iso B with a pentadentate EDTA coexists and contributes to the experimental spectrum as well.

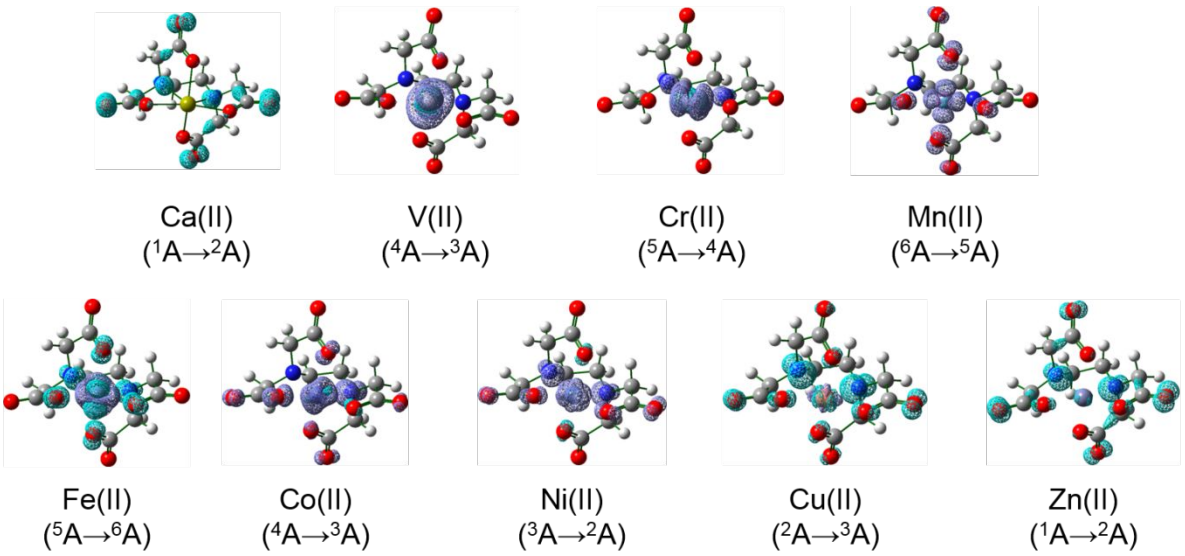

Fig. 4 Electron spin density differences between $[EDTA•M(III)]^-$ and $[EDTA•M(II)]^{2-}$ calculated at the optimized dianion's geometries based on Mulliken population analysis (Isovalue = 0.01). The detachment transition for each doubly charged complex is also noted.

C. Anti-correlation between electron detachment energy and *d* component in HOMO

The PE spectra in Figure 1 provide explicit electronic structure information on $[EDTA•M]^{2-}$. Peak X at the low eBE side is seen in the spectrum of each *M* = Mn, Co, Ni, Cu and Zn complex that formally contains 3d electrons, while is missing for *M* = Ca in which no d electrons are involved. Similar observation was reported recently in the PES study on $[EDTA•M(III)]^-$ (*M* = Al, Sc, and V− Co).[35] The VDE of the *TM*-EDTA complex, measured from the X band, increases in the order of Mn < Co < Ni < Cu < Zn, with the highest VDE of Ca-EDTA complex measured from the A band. To obtain a qualitative picture on where the least bound electrons being detached, electron spin density differences between $[EDTA•M]^-$ anions and $[EDTA•M]^{2-}$ dianions at the optimized dianionic geometries were computed based on

Mulliken population analyses (Figure 4). A salient feature is that the electron is entirely detached from the O atoms of EDTA ligand for $[EDTA•Ca]^{2-}$, whereas, for *TM* = V−Zn with d electrons, detachment is derived significantly from V(II) – Cu (II) metal cores, and noticeably from Zn(II), which has a d^{10} configuration. Molecular orbital (MO) analyses of the highest occupied (HO) MOs (Fig. S2) should further lead to insightful information on the nature of the detachment process to remove the least bound electrons. As listed in Table 2 and plotted in Figure 5, there exists a remarkable anti-correlation between the metal contribution in HOMOs and the VDEs across the entire $[EDTA•M(II)]^{2-}$ series. A similar anti-correlation between metal % in HOMOs and VDEs was also observed in photodetaching $[EDTA•M(III)]^{-}$ (M = Al, Sc, V−Co) as well.[35]

Table 2 Molecular orbital analyses of $[EDTA•M(II)]^{2-}$ (*M* = Ca, V−Zn) HOMOs, and the correlation between metal components in HOMOs and experimental / calculated VDEs.

$[EDTA•M(II)]^{2-}$	Ca(II)	V(II)	Cr(II)	Mn(II)	Fe(II)	Co(II)	Ni(II)	Cu(II)	Zn(II)
Exp. (VDE) (eV)	2.70			1.15		1.70	1.73	1.78	2.20
Theo. VDE (eV)	2.33	-0.42	0.16	1.16	0.64	1.64	1.63	1.66	2.08
Metal atoms (%)	0.80	85.60	69.70	50.70	84.10	22.90	22.20	12.70	2.70
N atoms (%)	27.30	0.20	15.80	3.80	0.50	31.90	28.80	38.30	29.00
O atoms (%)	45.30	9.50	8.70	42.10	13.90	32.40	37.90	30.20	47.60
C atoms (%)	20.20	3.90	2.50	2.50	2.00	7.10	6.20	11.00	14.40

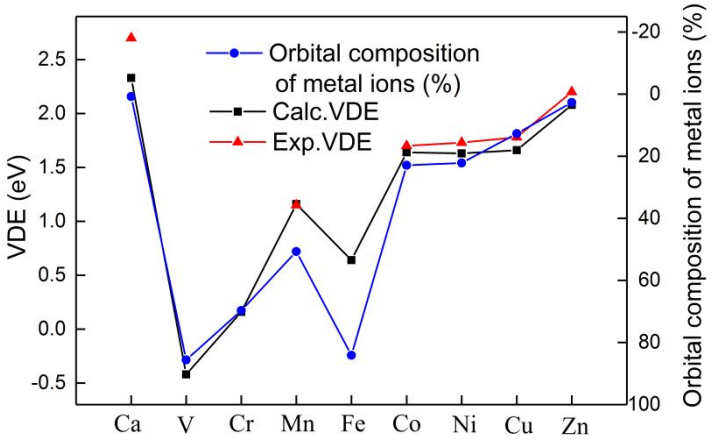

Fig. 5 The comparison of metal atom HOMO composition (%) with the experimental / calculated VDEs for complexes [EDTA•*M*(II)]$^{2-}$ (*M* = Ca, V−Zn). The percentage of the Cr composition in HOMO is set to equal to the calculated VDE.

D. Interconnections among gas phase VDEs, solution phase redox potentials, and third ionization potentials of metals

The half-reaction [EDTA•*M*(II)]$^{2-}$(*aq*) → [EDTA•*M*(III)]$^{-}$(*aq*) + *e* is a textbook notion for oxidation of [EDTA•*M*(II)]$^{2-}$ complexes in aqueous solutions. As such, the solution phase oxidation potential, $E_{1/2}$, should have natural connections with gas phase photodetachment and the 3rd ionization potential (IP) of *TM* atom.

The gas phase VDEs of [EDTA•*M*(II)]$^{2-}$ (red and blue triangles) are first compared to the 3rd IPs of metal *M* (green squares)[43] in Figure 6. A reasonable correlation is found between the VDE trend and that of the 3rd IPs for *M* = V, Cr, Mn, Fe, although their absolute numbers are different. The VDE reaches a plateau of 1.7 eV for the M = Co, Ni, Cu complexes, and 2.0 eV for the Zn, while the 3rd IP of the corresponding metal is seen to continue increasing. The good correlation between VDE and metal 3rd IP found for the *M* = V, Cr, Mn, Fe cases can be qualitatively explained by examining their HOMO components of these complexes, which shows that the metal core contributes dominantly to each HOMO in the V, Cr, Mn, and Fe complexes (Table 2). In contrast, ligand EDTA contributes overwhelmingly to each HOMO in the Co, Ni, Cu and Zn EDTA complexes, and therefore exhibits remarkable non-innocence and modulation ability for electron removal process,[44] a fact that rationalizes the deviation of VDE vs IP observed in these late *TM* complexes.

Figure 6 also compares the solution phase redox potentials $E_{1/2}$ (brown squares)[45] with the calculated / experimental VDEs for [EDTA•*M*(II)]$^{2-}$ (*M* = V – Co). The overall in-track of VDE with $E_{1/2}$, as was also reported in several other systems,[37, 46] suggests that the solvation energies for these quasi-octahedral structures are similar. A noticeable exception is found for the Co vs Mn cases, in which $E_{1/2}$ of the Co complex is smaller than that of Mn, but VDE of the former is higher than the latter. A close examination of the HOMO of each complex may provide a clue. The HOMO of [EDTA•Mn(II)]$^{2-}$ is largely comprised of the metal (50.70%), so the

electron removal process can be viewed as $[EDTA•Mn(II)]^{2-} \rightarrow [EDTA•Mn(III)]^{-}$. On the contrary, the HOMO of $[EDTA•Co(II)]^{2-}$ only has 23% Co contribution, so the electron removal process for this complex is better described as $[EDTA•Co(II)]^{2-} \rightarrow [EDTA^{+}•Co(II)]^{-}$. It is not surprising that the solvation energy for the Mn(II)/Mn(III) pair is different from the EDTA/EDTA^{+}, leading to the observed VDE vs $E_{1/2}$ deviation for these two complexes. The critical role of solvation energy that could change the VDE vs $E_{1/2}$ trend over a series of homologues compounds was also reported previously in investigating the electronic properties of various functionalized fullerenes.[47]

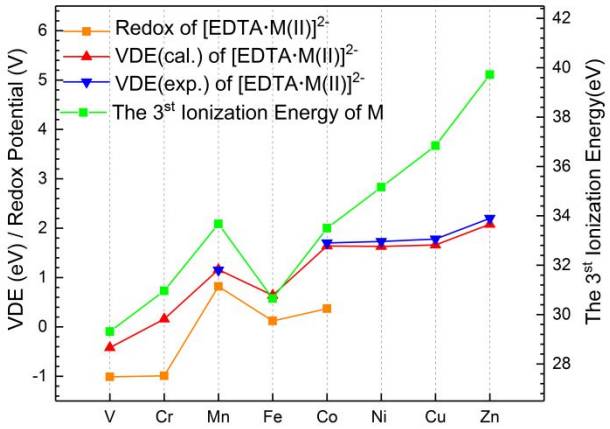

Fig. 6 Comparative trends among solution phase redox potentials (V, in volt), gas-phase VDEs for $[EDTA•M(II)]^{2-}$ (M = V−Zn) complexes (eV), and the 3rd ionization potentials (IP) of metal M (eV). The 3rd IP of Fe is set to equal to the calculated VDE of the Fe complex, and the scale ratio of the 3rd IP over VDE is set to 2/1.

Conclusion and perspectives

We have conducted a systematic investigation by employing electrospray ionization PES and quantum computations on a series of divalent metal EDTA complexes $[EDTA•M(II)]^{2-}$ across the 3rd row metals (M = Ca, V− Zn). The electronic origin regarding the redox nature of these divalent *TM* EDTA complexes is unraveled in their PE spectra, in which there is an extra spectral band X with the lowest eBE exhibited, when compared to that of $[EDTA•Ca(II)]^{2-}$. This X band is largely derived from the metal core for the early TM complexes, with significant EDTA contribution for the late TM species. Our DFT calculations suggest pseudo-octahedral

structures for all complexes, and the calculated VDEs are in good agreement with the experimental measurements. In addition, we compare the gas-phase VDEs with those corresponding solution redox potentials and 3rd IPs of the metals for this series of complexes. Overall good correlations among these three sets of data are found for those species with their HOMOs largely composed of TMs. Noticeable deviation between VDEs and IPs occurs when the EDTA ligand significantly contributes to redox active orbitals, and the VDE − redox potential relationship may break down when the respective solvation energy varies appreciably along the series. The in-depth analysis of the results obtained in this work, and those reported in our previous studies, has demonstrated that electrospray ionization PES is indeed a unique ion spectroscopic tool that has certain predictive power to foresee related redox chemistries over a series of structurally and compositionally similar compounds. However, cautions must be practiced in the cases where solvation energy or the properties of redox active orbitals change appreciably.

Conflicts of interest

The authors declare no conflicts of interest.

Acknowledgements

The experimental work was supported by the U.S. Department of Energy (DOE), Office of Science, Office of Basic Energy Sciences, Division of Chemical Sciences, Geosciences and Biosciences, and was performed using EMSL, a national scientific user facility sponsored by DOE's Office of Biological and Environmental Research and located at Pacific Northwest National Laboratory, which is operated by Battelle Memorial Institute for the DOE. The computational work was supported by the National Natural Science Foundation of China (Grant No. 21688102) and the Strategic Priority Research Program (Grant No. XDB17000000) of the Chinese Academy of Science and conducted on the clusters of the Center for Theoretical and Computational Chemistry at Dalian Institute of Chemical Physics.

ASSOCIATED CONTENT

Electronic supplementary information (ESI) available:

Comparison of the experimental VDE values to the calculated ones obtained using different functionals for [EDTA*M* (II)]$^{2-}$ (*M* = Mn, Co, Ni, Cu, and Zn) (Table S1); Comparison of relative energies for the hexadentate [EDTA•*M*(II)]$^{2-}$ (*M* = Mn, Co, and Ni) complexes of different spin states at the MN12SX/6-311+G(d,p) level (Table S2); Comparison of relative energies of different isomers for the [EDTA•*M*(II)]$^{2-}$ (*M* = Ca, V – Zn) complexes at the MN12SX/6-311+G(d,p) level (Table S3); Energy barriers for Iso A transforming into Iso B of the [EDTA•*M*(II)]$^{2-}$ (*M* = Ca, Mn, Co, Ni, Cu, and Zn) complexes at the MN12SX/6-311+G(d,p) level (Table S4); Schematic potential energy curves explaining the observed RCB effects on photoelectron spectra (Fig. S1); Atom contribution (%) of the *M*, N, O and C in the HOMO pictures of the most stable isomers of [EDTA•*M*(II)]$^{2-}$ (*M* = Ca, V−Zn) (Fig. S2); Cartesian coordinates for the optimized structures of [EDTA•*M*(II)]$^{2-}$ (*M* = Ca, V−Zn) (total 50 pages).

References

(1) A. Y. Louie and T. J. Meade, *Chem. Rev.*, 1999, **99**, 2711-2734.

(2) N. Raman, L. Mitu, A. Sakthivel and M. Pandi, *J. Iran. Chem. Soc.*, 2009, **6**, 738-748.

(3) K. D. Karlin, *Science*, 1993, **261**, 701-708.

(4) U. Jungwirth, C. R. Kowol, B. K. Keppler, C. G. Hartinger, W. Berger and P. Heffeter, *Antioxid. Redox Signal.*, 2011, **15**, 1085-1127.

(5) J. C. Joyner, J. Reichfield and J. Cowan, *J. Am. Chem. Soc.*, 2011, **133**, 15613-15626.

(6) N. Aoki, Y. Ishii, K. Tateda, T. Saga, S. Kimura, Y. Kikuchi, T. Kobayashi, Y. Tanabe, H. Tsukada and F. Gejyo, *Antimicrob. Agents Chemother.*, 2010, **54**, 4582-4588.

(7) J. Rosenberg, Y. Tashima, B. Horecker and S. Pontremoli, *Arch. Biochem. Biophys.*, 1973, **154**, 283-291.

(8) R. A. Fernandes, A. L. Daniel-da-Silva, A. P. Tavares and A. M. Xavier, *Chem. Eng. Sci.*, 2017, **158**, 599-605.

(9) H. Han and P. B. Dervan, *Proc. Natl. Acad. Sci.*, 1994, **91**, 4955-4959.

(10) R. P. Hertzberg and P. B. Dervan, *Biochem.*, 1984, **23**, 3934-3945.

(11) D. T. Sawyer and J. E. Tackett, *J. Am. Chem. Soc.*, 1963, **85**, 2390-2394.

(12) J. Friedly, D. Kent and J. Davis, *Environ. Sci. Technol.*, 2002, **36**, 355-363.

(13) K. Krishnan and R. A. Plane, *J. Am. Chem. Soc.*, 1968, **90**, 3195-3200.

(14) B. Nowack and L. Sigg, *J. Colloid Interface Sci.*, 1996, **177**, 106-121.

(15) A. McConnell, R. Nuttall and D. Stalker, *Talanta*, 1978, **25**, 425-434.

(16) J. Oakes and E. G. Smith, *J. Chem. Soc., Perkin Trans. 1*, 1983, **79**, 543-552.

(17) D. T. Sawyer and P. J. Paulsen, *J. Am. Chem. Soc.*, 1959, **81**, 816-820.

(18) T. M. Alam and R. A. Assink, *Magn. Reson. Chem.*, 1997, **35**, 427-431.

(19) S. Aime, R. Gobetto, R. Nano and E. Santucci, *Inorg. Chim. Acta*, 198**7**, **129**, L23-L25.

(20) B. Barnett and V. Uchtman, *Inorg. Chem.*, 1979, **18**, 2674-2678.

(21) M. Zabel, A. Poznyak and V. Pawlowski, *J. Struct. Chem.*, 2006, **47**, 581-584.

(22) E. Faulques, D. L. Perry, S. Lott, J. Zubkowski and E. Valente, *Spectrochim. Acta, Part A*, 1998, **54**, 869-878.

(23) R. Nuttall and D. Stalker, *Talanta*, 1977, **24**, 355-360.

(24) K. R. Asmis and D. M. Neumark, *Acc. Chem. Res.*, 2011, **45**, 43-52.

(25) N. Heine and K. R. Asmis, *Int. Rev. Phys. Chem.*, 2015, **34**, 1-34.

(26) F. S. Menges, S. M. Craig, N. Tötsch, A. Bloomfield, S. Ghosh, H. J. Krüger and M. A. Johnson, *Angew. Chem.*, 2016, **128**, 1304-1307.

(27) J. P. Wagner, D. C. McDonald and M. A. Duncan, *Angew. Chem. Int. Ed.*, 2018, **57**, 5081-5085.

(28) X.-B. Wang, *J. Phys. Chem. A*, 2017, **121**, 1389-1401.

(29) A. Sen, G.-L. Hou, X.-B. Wang and C. E. Dessent, *J. Phys. Chem. B*, 2015, **119**, 11626-11631.

(30) E. Garand, *J. Phys. Chem. A*, 2018, **122**, 6479-6490.

(31) J. N. Bull and J. R. Verlet, *Phys. Chem. Chem. Phys.*, 2017, **19**, 26589-26595.

(32) E. Matthews and C. E. Dessent, *Phys. Chem. Chem. Phys.*, 2017, **19**, 17434-17440.

(33) L. Giacomozzi, C. Kjær, J. Langeland Knudsen, L. Andersen, S. Brøndsted Nielsen and M. H. Stockett, *J. Chem. Phys.*, 2018, **148**, 214309.

(34) X.-B. Wang and L.-S. Wang, *J. Chem. Phys.*, 2000, **112**, 6959-6962.

(35) Q. Yuan, X.-T. Kong, G.-L. Hou, L. Jiang and X.-B. Wang, *Phys. Chem. Chem. Phys.*, 2018, **20**, 19458-19469.

(36) D. Hanstorp and M. Gustafsson, *J. Phys. B: At., Mol. Opt. Phys.*, 1992, **25**, 1773.

(37) X.-B. Wang and L.-S. Wang, *J. Chem. Phys.*, 1999, **111**, 4497-4509.

(38) X.-B. Wang, Y.-L. Wang, J. Yang, X.-P. Xing, J. Li and L.-S. Wang, *J. Am. Chem. Soc.*, 2009, **131**, 16368-16370.

(39) R. A. Gaussian09, *Inc., Wallingford CT*, 2009, **121**, 150-166.

(40) X.-B. Wang and L.-S. Wang, *Annu. Rev. Phys. Chem.*, 2009, **60**, 105-126.

(41) L.-S. Wang and X.-B. Wang, *J. Phys. Chem. A*, 2000, **104**, 1978-1990.

(42) J. N. Bull, C. W. West and J. R. Verlet, *Phys. Chem. Chem. Phys.*, 2015, **17**, 32464-32471.

(43) D. R. Lide, *CRC handbook of chemistry and physics*, CRC Boca Raton, 2012.

(44) X. Liu, G.-L. Hou, X. Wang and X.-B. Wang, *J. Phys. Chem. A*, 2016, **120**, 2854-2862.

(45) H. Ogino, T. Nagata and K. Ogino, *Inorg. Chem.*, 1989, **28**, 3656-3659.

(46) J. Warneke, S. Z. Konieczka, G.-L. Hou, E. Aprà, C. Kerpen, F. Keppner, T. C. Schäfer, M. Deckert, Z. Yang and E. Bylaska, *Phys. Chem. Chem. Phys.*, **2018**, DOI: 10.1039/C8CP05313H.

(47) I. V. Kuvychko, J. B. Whitaker, B. W. Larson, T. C. Folsom, N. B. Shustova, S. M. Avdoshenko, Y.-S. Chen, H. Wen, X.-B. Wang and L. Dunsch, *Chem. Sci.*, 2012, **3**, 1399-1407.

TOC

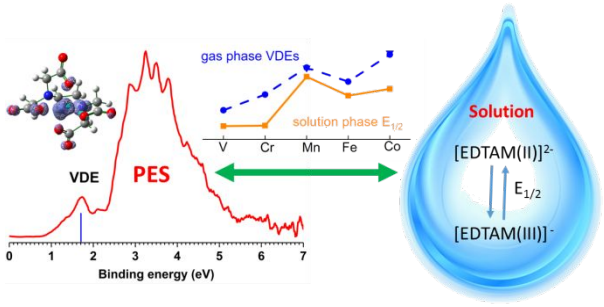

A systematic photoelectron spectroscopy and theoretical study of divalent transition metal EDTA complexes illustrates intrinsic correlations of redox properties in the gas and solution phases